Laser and Particle Beams (2009), *27*, 223–231. Printed in the USA.

doi:10.1017/S0263034609000299

Observation of quasi mono-energetic electron bunches in the new ellipsoid cavity model

R. SADIGHI-BONABI,[1] H.A. NAVID,[1] AND P. ZOBDEH[2]

[1]Department of Physics, Sharif University of Technology, Tehran, Iran
[2]Department of Physics, Amirkabir University of Technology, Tehran, Iran

(RECEIVED 18 November 2008; ACCEPTED 9 December 2008)

Abstract

In this work, we introduce a new ellipsoid model to describe bubble acceleration of electrons and discuss the required conditions of forming it. We have found that the electron trajectory is strongly related to background electron energy and cavity potential ratio. In the ellipsoid cavity regime, the quality of the electron beam is improved in contrast to other methods, such as that using periodic plasma wakefield, spherical cavity regime, and plasma channel guided acceleration. The trajectory of the electron motion can be described as hyperbola, parabola, or ellipsoid path. It is influenced by the position and energy of the electrons and the electrostatic potential of the cavity. In the experimental part of this work, a 20 TW power and 30 fs laser pulse was focused on a pulsed He gas jet. We have focused the laser pulse in the best matched point above the nozzle gas to obtain a stable ellipsoid bubble. The finding of the optimum points will be described in analytical details.

Keywords: Bubble regime; Intense laser; Laser wakefield; Plasma accelerator; Quasi mono-energetic electron bunches; Wave breaking

1. INTRODUCTION

In the last decade, the generation of laser pulses in the multi-terawatt (or even petawatt) power range is possible with compact chirped-pulse amplification (CPA) systems, and the extreme light infrastructure (ELI) will be able to generate intensities in the range of 10^{25}–10^{26} W/cm^2 (Gerstner, 2007). In CPA table-top lasers, the laser intensities increased up to $I = 10^{22}$ W/cm^2, and electric field strengths of more than 10^{14} V/m were obtained (Umstadter, 2003). Particles can be accelerated in these high gradient fields and used for various applications, including transmutation of cheep and hazardous materials of long-living radioactive wastes to valuable radioisotopes (Sadighi-Bonabi & Kokabee, 2006). The extremely high electric field makes the laser wakefield acceleration method attractive for the development of a new generation of accelerators (Geddes *et al.*, 2004). In the laser wakefield scheme, the ponderomotive force associated in the front and the rear sides of a short laser pulse expels the plasma electrons from the regions where the laser field is the most intense (Malka *et al.*, 2006). The induced charge separation between the electrons and the ions gives rise to a space charge field and a plasma wave (Robson *et al.*, 2007). Large amplitude plasma waves are generated by this ponderomotive force in the laser wakefield accelerator (LWFA). The ponderomotive force F_p is given by $F_p \approx -\nabla a^2$, where α is the laser pulse envelope. The acceleration gradient resulting from the charge displacement is reported to be about 100 GV/cm when plasma density is 10^{18} cm^{-3} (Hemker *et al.*, 2002).

In the linear regime, this mechanism is more efficient when the pulse duration of the laser is on the order of the plasma frequency, and it is called resonant wakefield. The resonant wakefield regime creates a controllable and linear accelerating structure. In nonlinear regimes, background plasma electrons can be trapped in the plasma wave bucket and accelerated up to GeV (Karmakar & Pukhov, 2007; Leemans *et al.*, 2006; Glinec *et al.*, 2005; Koyama *et al.*, 2006; Lifshitz *et al.*, 2006). One of the most important applications for such short ultra-intense laser pulses is the acceleration of charged particles, both electrons and ions (Flippo *et al.*, 2007; Hegelich *et al.*, 2006; Yin *et al.*, 2006; Roth *et al.*, 2005; Nickles *et al.*, 2007; Ruhl *et al.*, 2006). The self-modulated laser wakefield (SMLWF) (Esarey *et al.*, 1994)

Address correspondence and reprint requests to: R. Sadighi-Bonabi, Department of Physics, Sharif University of Technology, 11365-9567, Tehran, Iran. E-mail: sadighi@sharif.ir

and the forced laser wakefield (FLWF) (Malka *et al.*, 2002) are the well known nonlinear regimes. In the SMLWF regime, the envelope of the laser pulse can modulate at the plasma wave period and drives the wakefield properly with its ponderomotive force *via* Raman forward scattering instability. In the FLWF regime, the laser pulse is compressed by group velocity dispersion during the excitation of the plasma wave, and drives the plasma wave to very high amplitude. To obtain accelerated electrons with higher efficiencies, the electrons should be injected in the correct phase of the plasma wave. There the injection of background plasma electrons is possible instead of an external electron injector (e.g., a lilac) when wave-breaking occurs (Tomassini *et al.*, 2004). By using the steepened density profile, the wave-breaking injection can be fast. A well collimated, ultra short MeV electron bunch is obtained due to the transverse wave breaking (Zobdeh *et al.*, 2008*b*, 2008*c*, 2008*d*) by using a shock wave driven with the irradiation of laser prepulse (Hosokai *et al.*, 2006). In recent experiments and PIC simulations (Malka *et al.*, 2006), generation of quasi-monoenergetic electrons has been reported, A free cold plasma electrons cavity (bubble) behind the laser pulse is observed (Faure *et al.*, 2004). The following features are absent in the ordinary regime of laser wakefield acceleration (Kostyukov *et al.*, 2004; Gordienko & Pukhov, 2005; Esarey *et al.*, 1996; Pukhov *et al.*, 2004): (1) a cavity free from cold plasma electrons is formed behind the laser pulse instead of a periodic plasma wave; (2) a dense bunch of relativistic electrons with a quasi-monoenergetic spectrum is self-generated; (3) the laser pulse propagates many Rayleigh lengths in the homogeneous plasma without a significant diffraction. The cavity behind the laser pulse is shown by shadowgraphs (Mangles *et al.*, 2006) and PIC simulation (Pukhov & Meyer-ter Vehn, 2002; Faure *et al.*, 2004). Quasi-monoenergetic electron beams were generated from intense laser pulses in various gas targets (Chen *et al.*, 2008).

In this work, we describe analytically the new ellipsoid model (Zobdeh *et al.*, 2008*a*) to be used instead of the previous spherical cavity. In fact, the cavity shape is not exactly a sphere, and this is a defect in previous works (Gordienko & Puhkov, 2005; Kostyukov *et al.*, 2004). Some deviations between shadowgraphs, PIC simulation, and analytical calculation results are reported because of the spherical estimation for the cavity shape. Appropriate conditions of forming an ellipsoid cavity are obtained. We have evaluated fields inside of this cavity and the energy spectrum for relativistic trapped electrons, and obtain energy and electron gain when self-focusing is considered. In the experimental part of this work, a 20 TW power and 30 fs laser pulse was focused on a pulsed He gas jet (Sadighi-Bonabi & Zobdeh, 2008). We have focused the laser pulse in the best matched point above the nozzle gas to obtain a stable ellipsoid bubble. How to find the optimum point will be described in analytical details.

2. CAVITY STABILITY AND THE ELECTRON TRAJECTORY

Considering in the electron dynamic equation the internal electromagnetic fields and the ponderomotive force of the laser propagation, we obtain:

$$\ddot{r}\hat{r} = (\ddot{r} - r\dot{\theta}^2)\hat{r} + \frac{1}{r}\frac{d}{dt}(r^2\dot{\theta})\hat{\theta} = \frac{1}{\mu}\left(\frac{-eQ_i}{4\pi\varepsilon_0 r^2}\hat{r} + E_P\hat{\theta}\right), \quad (1)$$

where E_p, μ, r, $\dot{r}$, θ, $\dot{\theta}$, Q_i, e, and ε_0 are ponderomotive force, electron mass with approximately laser group velocity, radial component, derivative of radial component, tangential component, derivative of tangential component, average ion charge in the cavity, electron charge, and cavity dielectric constant, respectively. Eq. (1) can be separated into radial and tangential components. We can assume for the electron motion on the cavity sheath that the radius vector r sweeps out an angle $d\theta$ in a short time dt. If A is defined as the area swept, then we have $dA = (1/2)r^2\, d\theta$, $dA/dt = (1/2)r^2\dot{\theta}$. We, as usual, define the system's constant angular momentum by $\ell = |L| = \mu r^2\dot{\theta}$. So, one has

$$\dot{\theta} = \frac{\ell}{\mu r^2}, \text{ and } \frac{dA}{dt} = \frac{\ell}{2\mu} = const.,$$

then,

$$\ddot{r} = r\dot{\theta}^2 - \left(\frac{e}{\mu}\frac{Q_i}{4\pi\varepsilon_0 r^2}\right) = \frac{\ell^2}{\mu^2 r^3} - \left(\frac{e}{\mu}\cdot\frac{Q_i}{4\pi\varepsilon_0 r^2}\right). \quad (2)$$

We assume that the solution $r(t)$ can be written as $r = r(\theta)$, where $\theta = \theta(t)$. Then we seek a solution in the form $u(r) = 1/r(\theta(t))$:

$$\dot{r} = \frac{dr}{dt} = \frac{dr}{du}\frac{du}{dt} = \frac{dr}{du}\frac{du}{d\theta}\frac{d\theta}{dt}.$$

Recalling that $\ell = \mu r^2\dot{\theta}$ and $r = 1/u$, we have

$$\dot{r} = -\frac{1}{u^2}\frac{du}{d\theta}\frac{\ell}{\mu r^2} = -\frac{\ell}{\mu}\cdot\frac{du}{d\theta}.$$

It follows

$$\begin{aligned}\ddot{r} &= -\frac{\ell}{\mu}\frac{d}{dt}\left(\frac{du}{d\theta}\right) = -\frac{\ell}{\mu}\frac{d^2u}{d\theta^2}\frac{d\theta}{dt} = -\frac{\ell^2}{\mu^2}u^2\frac{d^2u}{d\theta^2} \\ &= \frac{\ell^2}{\mu^2}u^3 - ku^2,\end{aligned} \quad (3)$$

where $k = -e/\mu\cdot Q_i/4\pi \in_0$,

$$\frac{d^2u}{d\theta^2} + u = \frac{1}{\alpha}, \quad (4)$$

https://doi.org/10.1017/S0263034609000299 Published online by Cambridge University Press

with

$$\frac{1}{\alpha} = \frac{k\mu^2}{\ell^2} = -\frac{e\mu}{\ell^2}\frac{Q_i}{4\pi \in_0},$$
$$u(\theta) = A\cos\theta + \frac{1}{\alpha}, \tag{5}$$

so we get

$$r(\theta) = \frac{1}{u} = \frac{1}{A\cos\theta + 1/\alpha}. \tag{6}$$

Finally, if we set $A = \varepsilon/\alpha$, then: we obtain

$$r(\theta) = \frac{\alpha}{1 + \varepsilon\, \boldsymbol{cos}\theta}, \tag{7}$$

where α and ε are constant. Similar considerations and derivations may also be found in classical dynamics of particles and systems (Marion & Thornton, 1998).

From Eq. (7) follows, that the electron trajectory is a hyperbola if $\varepsilon > 1$, a parabola if $\varepsilon = 1$, an ellipse if $0 < \varepsilon < 1$, and a circle if $\varepsilon = 0$. This is shown in Figure 1. For the case of the ellipsoid trajectory ($\varepsilon \neq 1$ and $0 < \varepsilon < 1$), we define the length of the ellipse's long axis $= 2a_e$, then $2a_e = r(0) + r(\pi) = 2\alpha/1 - \varepsilon^2$ and $r(\theta) = a_e(1 - \varepsilon^2)/1 + \varepsilon\cos\theta$.

3. DISCUSSION OF THE TRAJECTORY

In Eq. (6), the constant "A" can be defined by the initial condition of the electron. It means the trajectory will depend strongly on the initial condition. For an electron far from the bubble, $\theta = 0$, $r \to \infty$, $r = \alpha/(1 + \cos\theta)$ one has a parabola as a trajectory. For the electron at the margin of the bubble at $\theta = 0$, $r = R$, it yields $r = \alpha/1 - ((\alpha/R) - 1)\cos\theta$, $(\alpha/R) \propto -(l^2/\mu R^2)/eQ_i/4\pi\varepsilon_0 R$, where R is the radius of the bubble, and α/R is proportional to the ratio of electron energy to electrostatic energy. So the electron trajectory will depend on α/R. The electron has a circular trajectory if $(\alpha/R) - 1 = 0$, or $\alpha/R = 1$. The electron has an ellipse trajectory if $0 < (\alpha/R) - 1 < 1$, or $1 < (\alpha/R) < 2$. The electron trajectory is influenced by its position and energy, and the electrostatic potential of the cavity.

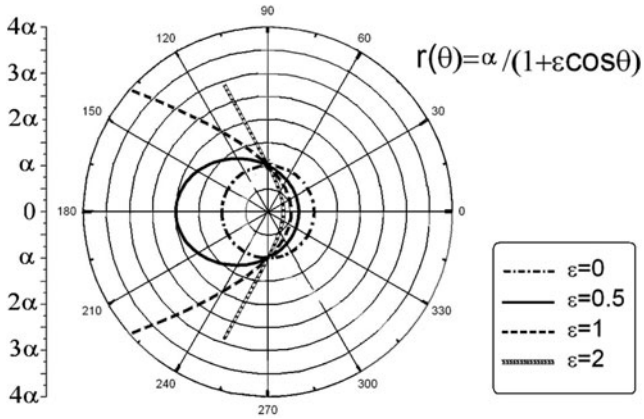

Fig. 1. Electron trajectory for different eccentricities ε: hyperbola if $\varepsilon > 1$, parabola if $\varepsilon = 1$, ellipse if $0 < \varepsilon < 1$ and circle if $\varepsilon = 0$.

4. ELECTROMAGNETIC FIELDS AND ELECTRON ENERGY INSIDE THE CAVITY

We consider a cavity moving in plasma. Ions are immobile in the cavity while the cavity runs with the relativistic velocity $v_0 \approx 1$ along the x-axis. The ion dynamics are neglected because the cavity dimensions are assumed to be smaller than the ion response length $\approx c/\omega_{pi}$, where $\omega_{pi} = (4\pi e^2 n_0/M)$ is the ion plasma frequency, and M is the ion mass. To calculate the fields, we write the Maxwell equations in terms of potentials using the following convenient gauge $A_x = -\varphi$. According to the calculations of Kostyukov *et al.* (2004) we get:

$$\Delta = 1 - n\left(1 - \frac{p_x}{\gamma}\right) + \left(\frac{\partial}{\partial t} + \frac{\partial}{\partial x}\right)(\nabla \cdot \boldsymbol{A}) + \frac{1}{2}\frac{\partial}{\partial t}\left(\frac{\partial}{\partial t} - \frac{\partial}{\partial x}\right)\Phi, \tag{8}$$

$$\nabla \times \nabla \times \boldsymbol{A} + n\frac{\boldsymbol{p}}{\gamma} + \frac{\partial}{\partial t}\left(\frac{\partial \boldsymbol{A}}{\partial t} - \frac{\nabla\Phi}{2}\right) = 0. \tag{9}$$

Here we use the wakefield potential $\Phi = A_x - \varphi$ instead of the scalar one, and $\boldsymbol{p}$ is the electron momentum. We use dimensionless units, normalizing the time to ω_p^{-1}, the lengths to c/ω_p, the velocity to c, the electromagnetic fields to $mc\omega_p/|e|$ and the electron density n to the background density n_0. If we use a quasi-static approximation assuming that all quantities depend on $\xi = x - v_0 t$ instead of x and t.

$$\Delta\Phi = 2(1-n)\left[1 - \frac{v_0}{(1+v_0)^2}\right] + \frac{2v_0}{(1+v_0)^2}\frac{np_x}{\gamma} - \frac{2}{(1+v_0)}\frac{\partial}{\partial\xi}\nabla_\perp \cdot \boldsymbol{A}_\perp, \tag{10}$$

$$\Delta_\perp \boldsymbol{A}_\perp - \nabla_\perp(\nabla_\perp \cdot A_\perp) = n\frac{\boldsymbol{p}_\perp}{\gamma} + \nabla_\perp\left(\frac{\partial\Phi}{\partial\xi}\right) - (1 - v_0^2)\frac{\partial^2}{\partial\xi^2}\boldsymbol{A}_\perp. \tag{11}$$

Inside the cavity we assume ($n = 0$), then we get

$$\Delta\Phi = 2\left[1 - \frac{v_0}{(1+v_0)^2}\right] - \frac{2}{(1+v_0)}\frac{\partial}{\partial\xi}\nabla_\perp \cdot \boldsymbol{A}_\perp \tag{12}$$

https://doi.org/10.1017/S0263034609000299 Published online by Cambridge University Press

$$\Delta_\perp \boldsymbol{A}_\perp - \nabla_\perp(\nabla_\perp \cdot \boldsymbol{A}_\perp) = \nabla_\perp(\frac{\partial \Phi}{\partial \xi}) - (1 - \mathrm{v}_0^2)\frac{\partial^2}{\partial \xi^2}\boldsymbol{A}_\perp. \quad (13)$$

The solution of basic Maxwell Eqs. (9) and (10) inside an ellipsoid electron cavity is:

$$\Phi(\xi, y, z) = 1 + \frac{a^2}{(1+\mathrm{v}_0)^2}\left(\frac{\xi^2}{a^2} + \frac{y^2}{b^2} + \frac{z^2}{c^2} - 1\right),$$
$$A_x = -\phi = \frac{\Phi}{2}, \quad (14)$$

where

$$a^2 = \mathrm{v}_0(1+\mathrm{v}_0)\frac{b^2c^2}{b^2+c^2}. \quad (15)$$

We assumed that the potential on the surface of the ellipsoid is constant and $\Phi = 1$. Eq. (15) has an important result, which is one of the most attractive features of ellipsoid regime, and it is the elongation of the ellipsoid bubble in the direction of relativistic movement for the fixed amount of b and c axis of the ellipsoid.

Where a, b, and c are the semi-axes of the ellipsoid, with azimuthally symmetry about x axis we have:

$$\Phi = 1 + \frac{1}{(1+\mathrm{v}_0)^2}\left(\xi^2 + \frac{y^2+z^2}{a'^2} - a^2\right) \quad (16)$$

$a'^2 = 2/(\mathrm{v}_0\,(1+\mathrm{v}_0))$. Here the velocity of bubble is v_0 and contrary to Pukhov *et al.* (2004), we did not set $\mathrm{v}_0 = 1$. The electromagnetic fields inside the relativistic cavity are:

$$E_x = \frac{1}{1+\mathrm{v}_0}\xi,\ E_y = -B_z = \frac{1}{2}\frac{\mathrm{v}_0}{1+\mathrm{v}_0}y,$$
$$E_z = B_y = \frac{1}{2}\frac{\mathrm{v}_0}{1+\mathrm{v}_0}z,\ B_x = 0. \quad (17)$$

If we substitute $v_0 = 1$ then the model will reduce to the spherical regime.

As seen from the PIC results in Figure 2, it is evident that the slope of E_y is less than one-fourth, and it is inconsistent with Eq. (14) since we always have $\mathrm{v}_0 < 1$. The calculated distribution of electromagnetic fields is close to the one observed in the three-dimensional PIC simulation (Fig. 2). This was a defect of spherical model and it was mentioned earlier by Pukhov *et al.* (2004) and Kostyukov *et al.* (2004). The small deviation from the analytically calculated field distribution is because the cavity shape is not exactly a sphere (Pukhov *et al.*, 2004; Kostyukov *et al.*, 2004).

The Lorentz force acting on a relativistic electron with $\mathrm{v} = \mathrm{v}_x = \mathrm{v}_0$ inside the cavity is

$$F_x = -E_x = \frac{-1}{1+\mathrm{v}_0}\xi,\ F_y = -E_y + \mathrm{v}_0 B_x = -\frac{\mathrm{v}_0}{2}y,$$
$$F_z = -E_z - \mathrm{v}_0 B_y = \frac{-\mathrm{v}_0}{2}z \quad (18)$$

The wake potential Φ can be considered with $\mathrm{v}_x = \mathrm{v}_0$ as the potential of the Lorentz force on the electron. The Lorentz force with $\mathrm{v}_x = -\mathrm{v}_0$ is:

$$F_x = E_x = \frac{-1}{1+\mathrm{v}_0}\xi,\ F_y = -E_y - \mathrm{v}_0 B_x = -\frac{1}{2}\frac{\mathrm{v}_0(1-\mathrm{v}_0)}{1+\mathrm{v}_0}y,$$
$$F_z = -E_z + \mathrm{v}_0 B_y = -\frac{1}{2}\frac{\mathrm{v}_0(1-\mathrm{v}_0)}{1+\mathrm{v}_0}z. \quad (19)$$

The dynamics of electron acceleration in an ellipsoid cavity can be analyzed using the Hamiltonian formulation. The general one-dimensional Hamiltonian of a charged particle in an electromagnetic field is

$$H = \sqrt{1 + (p_c + A)^2 + a^2} - \mathrm{v}_0 p_c - \phi, \quad (20)$$

where p_c is the particle canonical momentum and φ is the scalar potential. The Hamiltonian can be split into two parts by expanding it in the power of p_c^2. The first part determines the longitudinal motion and the second part determines the transverse motion. We obtain the longitudinal Hamiltonian and consider only the x dimension

$$H_\parallel = \sqrt{1 + p_x^2 + a^2} - \mathrm{v}_0 p_x - (1+\mathrm{v}_0)\phi \approx 1 + \frac{1+\mathrm{v}_0}{2} \quad (21)$$

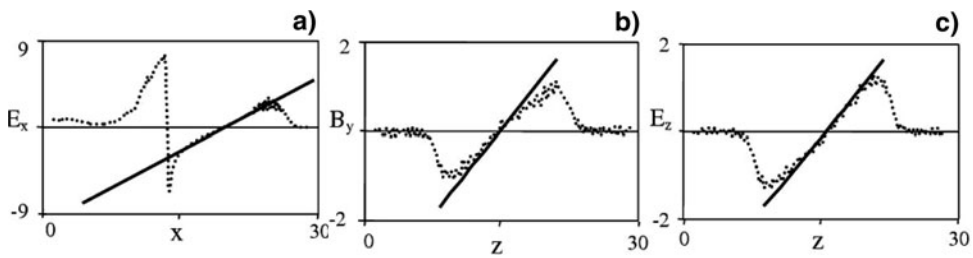

Fig. 2. Space distribution of the electromagnetic fields normalized to $mc\omega_p/|e|$ at the time instance when the laser pulse has passed $25c/\omega_p$: (**a**) E_x as a function of x; (**b**) B_y as a function of z; (**c**) E_z as a function of z. The PIC simulation results are shown by dashed lines while the analytical results are shown by solid lines. The coordinates are given in c/ω_p (Pukhov *et al.*, 2004).

https://doi.org/10.1017/S0263034609000299 Published online by Cambridge University Press

Here p_x is the momentum in the x direction. We have used the wake potential and the initial conditions $p_x = \alpha = 0$ and $\Phi = 1$ are applied. With the assumption $p_x \gg \gamma_0$ and $\alpha \approx 0$ this can be written as:

$$H_{\parallel} = \frac{p_x}{2\gamma_0} + \frac{1+v_0}{2}\left[1 + \frac{\xi^2 - a^2}{(1+v_0)^2}\right] \approx 1 + \frac{1+v_0}{2}. \quad (22)$$

The maximum energy of the accelerated electrons peaked at the cavity center is given by the following equation:

$$\gamma_{max} = 2\gamma_0^2\left[1 + \frac{a^2}{2(1+v_0)}\right]. \quad (23)$$

If we insert for a the value found from Eq. (15), then we get

$$\gamma_{max} = 2\gamma_0^2\left[1 + \frac{v_0}{2} \cdot \frac{b^2c^2}{b^2+c^2}\right]. \quad (24)$$

The result of this equation is very important. It shows that the maximum energy for a defined ellipsoid with fixed dimension along the y and z directions at higher speed of bubble increased due to the dependence of the energy on the bubble velocity. This is because of the dependence of the magnitude of a on v_0 and the elongation of the ellipsoid in the x direction Eq. (15). For $b = c$ we have

$$\gamma_{max} = 2\gamma_0^2\left[1 + \frac{v_0}{4}b^2\right]. \quad (25)$$

This is similar to the results of the spherical model by Pukhov *et al.* (2004).

As a consequence, we can see that the ellipsoid bubble model is the better representative of the relativistic electron energy. It shows that at higher speeds, the electrons will have higher energies. If $a = b = c$ and $v_0 = 1$ then Eqs (23) to (25) will be the same as in the spherical model of Pukhov *et al.* (2004). As a result, we can conclude that the spherical model is a special state of ellipsoid model introduced in this paper for the first time.

The initial condition to obtain an ellipsoid cavity is defined by the laser-plasma parameters. According to the previous discussion in Section 3, the electron trajectory is influenced by the ratio of its energy to the cavity electrostatic potential. When the ellipsoid cavity regime is obtained ($0 < \varepsilon < 1$), the electron energy in the ellipsoid cavity has a low spread spectrum and its maximum amount in the center depends on the semi-axis a elongation during the laser pulse propagation in experimental and PIC simulation results.

It follows that the electrons of the bunch have equal energy, and the ellipsoid cavity holds the electron bunch in a quasi-monoenergetic regime better than previous spherical models. In the spherical model, the energy of the accelerated electrons' peak is given by (Kostyukov *et al.*, 2004)

$$\gamma_{max} \approx \frac{1}{2}\gamma_0 R^2. \quad (26)$$

In this equation, R is the radius of the spherical bubble, and γ_0 is defined as $\gamma_0 = (1 - v_0)^{-1/2}$. v_0 is the laser pulse group velocity (Kostyukov *et al.*, 2004). Eq. (26) shows that the electron bunch energy is strongly related to the transverse radius of the cavity, and during the laser propagation, because of the longitudinal elongation of the cavity, the energy peak spectrum will spread. But in the ellipsoid model, according to Eq. (23), the longitudinal elongation (a) influences the energy spectrum of the electron bunch. This is an improved version of our previous works (Zobdeh *et al.*, 2008*b*, 2008*c*).

5. EXPERIMENTAL SETUP AND QUASI-MONOENERGETIC ELECTRON RESULT

In order to generate a laser acceleration wakefield, a 20 TW, 30 fs laser pulse based on the Ti-Sapphire CPA laser system has focused onto a supersonic He gas jet with a $f/5$ off-axis gold-coated parabolic mirror. The scheme of the experimental setup is shown in Figure 3. The focal spot size and the focusing location at different positions from the beginning of the gas jet are measured by using a charged coupled device (CCD) camera with a microscope objective lens. The typical spot size diameter was equal to 11 μm horizontally and 12 μm vertically at full width at half-maximum (FWHM) that is shown in Figure 4. The gas target stagnation pressure (plasma density) can be adjusted by a solenoid supersonic pulsed valve. The nozzle that produced the gas jet had a 2 mm cylindrical shape hole. The density distribution of the gas jet is measured by a Mach-Zehnder interferometer. The electron beam energies are detected by using a permanent magnet on image plates (Tanaka *et al.*, 2005; Hutchinson, 1987). We changed the laser power from 1 TW to 18 TW, and the plasma density from 2×10^{19} cm^{-3} to 14×10^{20} cm^{-3}. Most of the electron energy spectrums possess a Maxwellian distribution that is shown in Figure 5.

When the power of the laser was 16.6 TW (500 mJ) and the maximum density of the plasma amounted to 14×10^{19} cm^{-3}, we observed the quasi-monoenergetic electrons by focusing of the laser beam along the axis of laser propagation, which was one millimeter above the edge of the nozzle. By focusing of the laser beam at different positions from the beginning of gas jet (Fig. 3), we obtained various electron energy profiles. In this experiment, we did not observe any evidence of bubble formation resulting in monoenergetic electrons up to 200 ± 5 μm from the beginning of gas jet. At 250 ± 5 μm (at the point 1 of Fig. 6), we obtained quasi-monoenergetic electrons that are shown in Figure 7. Figure 6 show that one can obtain high energy electrons with narrower energy distribution by better and precise focusing. When we moved further along the laser beam, the profile of the electrons changed more to the quasi-Maxwellian

https://doi.org/10.1017/S0263034609000299 Published online by Cambridge University Press

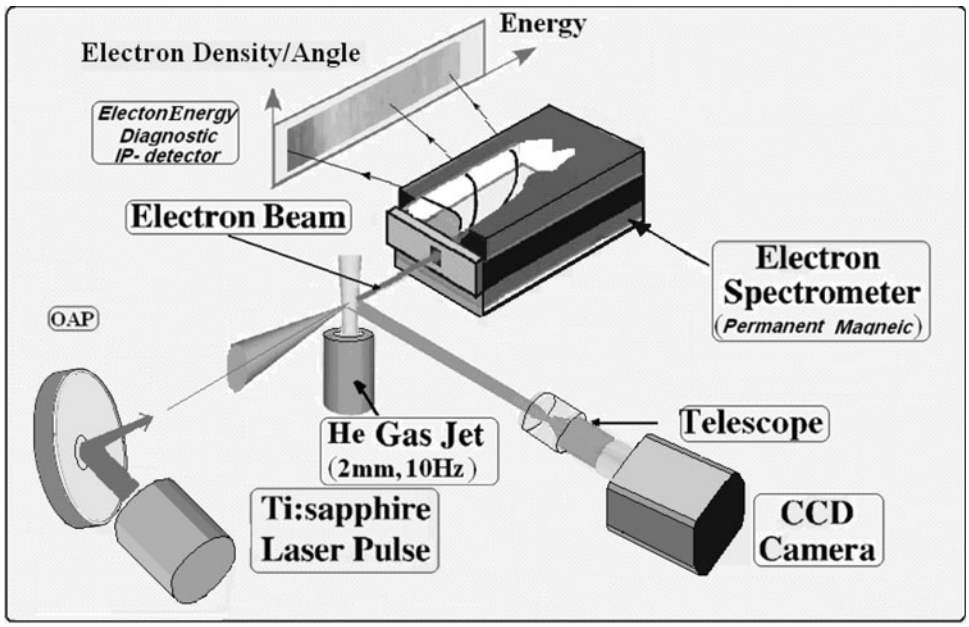

Fig. 3. The experimental setup is shown. The 30 fs laser pulse is focused into the He gas jet using the f/5 off-axis gold-coated parabolic mirror. The gas target density can be adjusted by a solenoid supersonic valve. Electron beam energies are detected by using a permanent magnet on the image plates.

shapes (at points 2 and 3 of Fig. 6). Under the conditions of this experiment (focusing radius of 5.5 μm), points less than 600 μm showed 100% distribution of electron energy as we can see in Figure 6.

6. DISCUSSION

For the condition of cavity formation, at the initial state of laser-plasma interaction, the ponderomotive potential of the laser pulses determines the cavity shape. If we assume the cavity

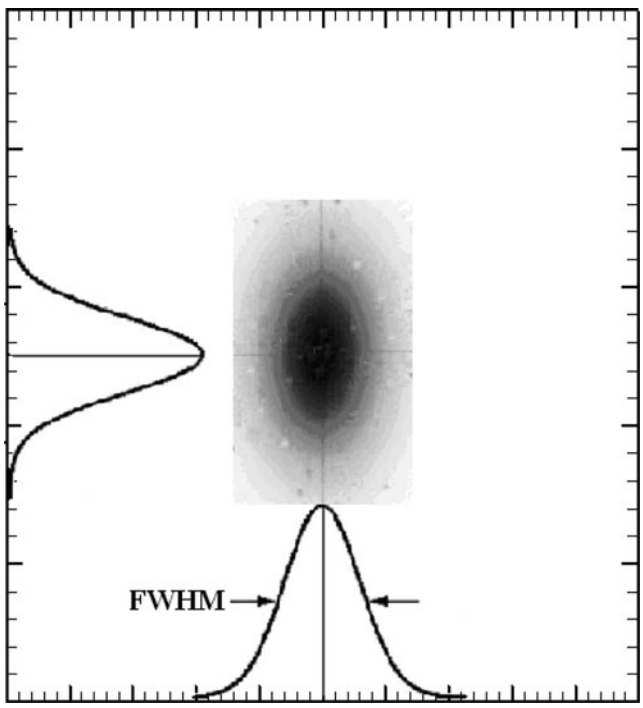

Fig. 4. Two dimensional of the laser beam distribution recorded by CCD camera. The typical horizontal and vertical dimensions of laser spot diameters at full width half-maximum (FWHM) were equal to 11 μm and 12 μm respectively.

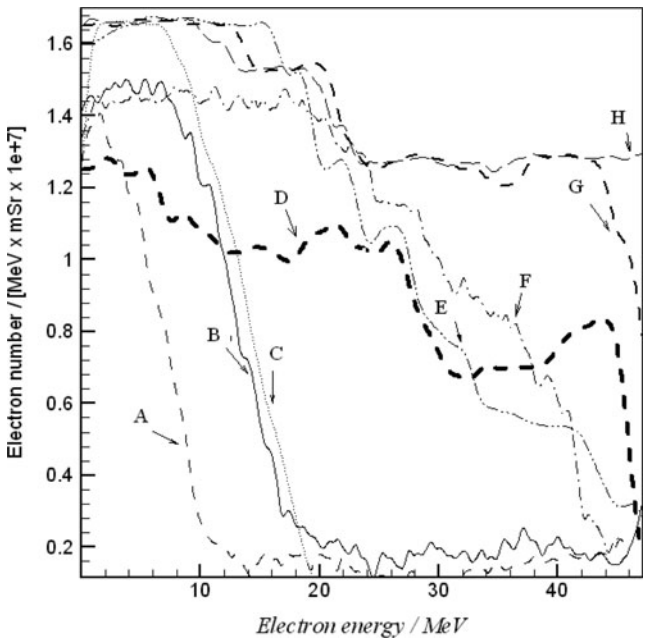

Fig. 5. Quasi-Maxwellian electron energy results at various laser powers and the maximum density of plasma density profiles, **A**: 1 *TW*, 2×10^{19} cm^{-3}, **B**: 3.5 *TW*, 3×10^{19} cm^{-3}, **C**: 4.4 *TW*, $4/5 \times 10^{19}$ cm^{-3}, **D**: 6.3 *TW*, 2.8×10^{20} cm^{-3}, **E**: 9.5 *TW*, 6.3×10^{20} cm^{-3}, **F**: 10.2 TW, 7.7×10^{20} cm^{-3}, **G**: 15.5 TW, 9.2×10^{20} cm^{-3}, **H**: 18 TW, 13.7×10^{20} cm^{-3}.

https://doi.org/10.1017/S0263034609000299 Published online by Cambridge University Press

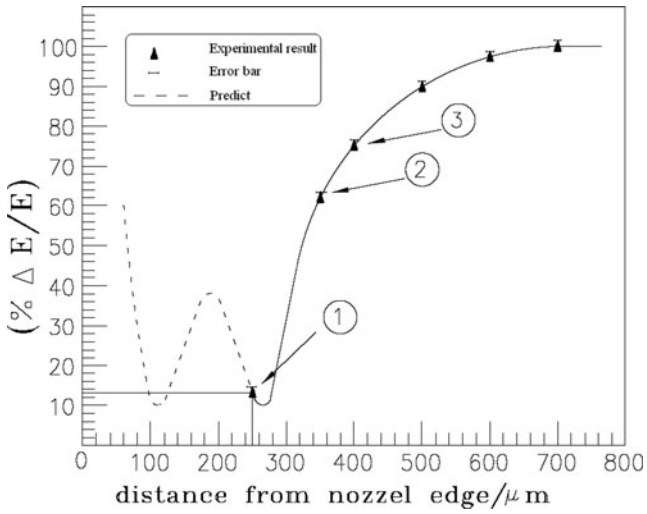

Fig. 6. Electron energy percentage distribution (% $\Delta E/E$), for different focused distances along the axis of laser propagation .The laser power is 16.6 TW and the maximum of the plasma density profile is 14×10^{19} cm^{-3}. The solid part of the curve is produced by experimental measurement and the dashed part is plotted from the predicted parameters of Figure 8.

shape in this situation to be a sphere, the electron sheath of the cavity feels the Lorentz force, which is nearly balanced by the laser ponderomotive force. The transverse radius R of the cavity can thus be estimated from the equation (Kostyukov *et al.*, 2004)

$$\frac{R}{4}(1-\mathrm{v}_x)\approx\frac{R}{4}\approx F_{pond}\approx\frac{\partial}{\partial R}\sqrt{1+a^2(R)}. \tag{27}$$

The ponderomotive force is written for the laser pulse which is spherical and circularly polarized. The electron kinetic energy is neglected when we compare it to the ponderomotive potential. For the laser pulse, at relativistic intensity, we have a Gaussian profile for the intensity distribution. The dimensionless amplitude $a(r)$ will be focused to a spot size ω_0 by a Gaussian profile (Gibbon, 2005)

$$a(r)=a_0\exp\left(-\frac{r^2}{2w_0^2}\right). \tag{28}$$

Substituting Eq. (28) into Eq. (27) and converting the dimensionless R to r, one obtains for the bubble radius

$$R=w_0\sqrt{\ln\frac{a_0\lambda_p}{w_0}}, \tag{29}$$

where λ_p is the wavelength of plasma. The effective ponderomotive potential is considered when the laser pulse length is on the order of half of the plasma wavelength. For the cavity regime condition, we also have $c\tau \le R$ (where τ is laser pulse duration). By consideration of SMLWFA, $c\tau = nR$ is the most stable cavity condition (Hidding *et al.*, 2006; Amthor,

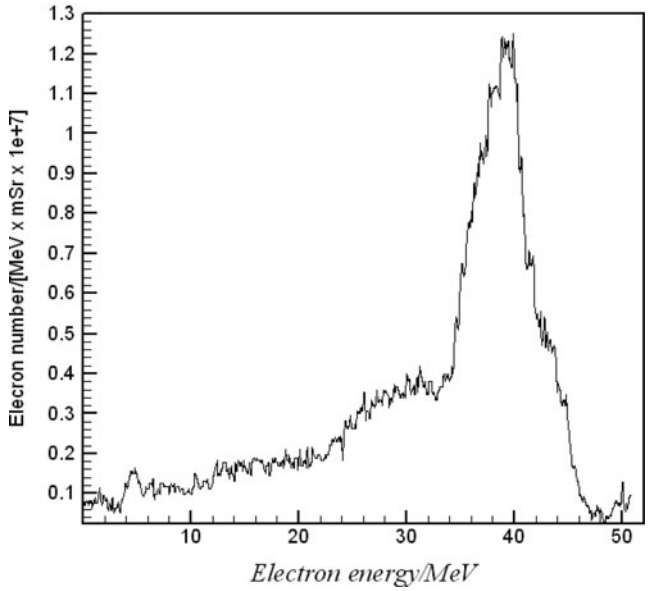

Fig. 7. The quasi-monoenergetic electron spectrum is shown. The laser power is 16.6 TW and the maximum of the plasma density profile is 14×10^{19} cm^{-3}. The laser beam was focused along the axis of laser propagation in 250 ± 5 μm distance 1 mm above the nozzle edge. The related image plate is shown at the top of the figure.

2006). So the stable condition can be obtained for $R = m\lambda p/2$, where n and m are positive integer numbers.

We have assumed a Gaussian plasma density distribution of the nozzle gas, and considered a slowly steepened profile with $n = Lz + n_0$ for the beginning regions of the plasma over the nozzle. Here L is a steepened plasma length and n_0 is the initial density. In this region, the wavelength of plasma will change as a function of $Lz + n_0$, and so the bubble radius may be calculated by Eq. (29). We

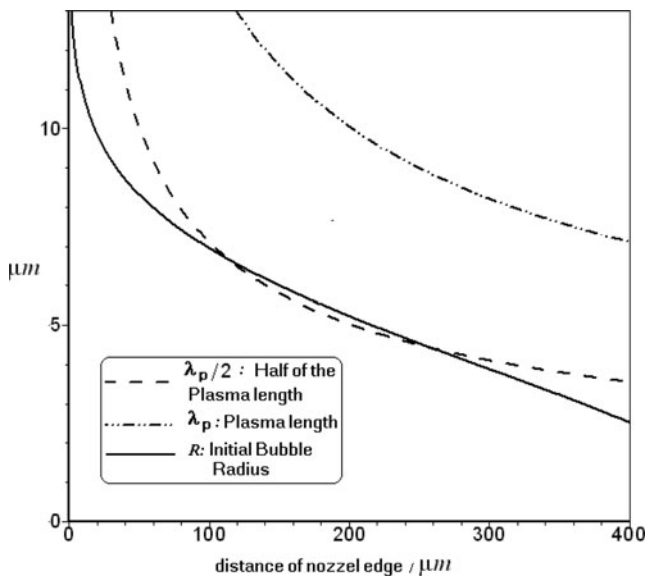

Fig. 8. The intersection points of $\lambda_p(z)/2$ and $R(z)$ are the optimum points to produce stable bubbles to trap monoenergetic electrons. No crossings exist between higher order multiples of $\lambda_p(z)/2$, e.g., $\lambda_p(z)$ and $R(z)$.

https://doi.org/10.1017/S0263034609000299 Published online by Cambridge University Press

have simulated this condition and shown that there are two particular points for laser focusing to obtain the optimum condition of cavity radius stability (Fig. 8).

We can conclude from Figure 8 that point 1 of Figure 6 corresponds to the bubble radius of only 4 μm, which is smaller than our 5.5 μm spot size radius. However, the first minimum point in Figure 6 corresponds to a bubble radius larger than 6.5 μm. Thus, we were not able to detect this point with our 5.5 μm laser beam spot size radius. Any distance shorter than the first minimum corresponds to a larger bubble radius, which we were unable to see. According to our aim to see larger bubbles to trap more electrons, we should produce larger laser spot sizes, which cause the reduction of our laser intensity below the critical relativistic intensities. As a result of that, to observe larger bubbles, one needs to have a laser beam with higher peak powers.

7. CONCLUSIONS

Previous cavity models such as the spherical model show some deviations in comparison with experimental and PIC results (Pukhov *et al.*, 2004). In this work, we have presented an analytical calculation of the new elliptical model for the first time. We have shown that the electron trajectory can have the form of a hyperbola, parabola, and ellipse, and there are initial and final conditions for the ellipsoid cavity formation. A dense bunch of relativistic electrons with monoenergetic spectrum is self-generated, and the fields depend linearly on the coordinates. We have shown that the cavity elongation with fixed b and c semi-axis affected the maximum electron energy, so the quality of the electron beam is improved.

Finally, based on our experiments and calculations, we conclude the following two essential points. (1) In a defined density profile, only defined points can produce mono-energetic electrons beam. (2) In order to observe bigger bubbles for trapping more electrons, one has to use laser beams with higher powers to obtain larger focal spots with intensities larger than the critical relativistic intensities.

ACKNOWLEDGMENTS

The authors acknowledge the ministry of oil (IRI) for partial support of this work through contract No.1211 by Pars Oil and Gas Company, also the constructive cooperation of Prof. J. Zhong from CAS is deeply appreciated.

REFERENCES

Amthor, K.-U. (2006). *Laser plasma accelerators for charged particles*. Ph.D. Thesis. Jena, Germany: Friedrich-Schiller-Universitaet Jena.

Chen, Z.L., Unick, C., Vafaei-Najafabadi, N., Tsui, Y.Y., Fedosejevs, R., Naseri, N., Masson-Laborde, P.E. & Rozmus, W. (2008). Quasi-monoenergetic electron beams generated from 7 TW laser pulses in N-2 and He gas targets. *Laser Part. Beams* **26**, 147–155.

Esarey, E., Krall, J. & Sprangle, P. (1994). Envelope analysis of intense laser pulse self-modulation in plasmas. *Phys. Rev. Lett.* **72**, 2887–2890.

Esarey, E., Sprangle, P., Krall, J. & Ting, A. (1996). Overview of plasma-based accelerator concepts. *IEEE Trans. Plasma Sci.* **24**, 252–288.

Faure, J., Glinec, Y., Pukhov, A., Kiselev, S., Gordienko, S., Lefebvre, E., Rousseau, J.P., Burgy, F. & Malka, V.A. (2004). Laser-plasma accelerator producing monoenergetic electron beams. *Nat.* **431**, 541–544.

Flippo, K., Hegelich, B.M., Albright, B.J., Yin, L., Gautier, D.C., Letzring, S., Schollmeier, M., Schreiber, J., Schulze, R. & Fernández, J.C. (2007). Laser-driven ion accelerators: spectral control, monoenergetic ions and new acceleration mechanisms. *Laser Part. Beams* **25**, 3–8.

Geddes, C.G.R., Toth, C.S., Van Tilborg, J., Esarey, E., Schroeder, C.B., Cary, J. & Leemans, W.P. (2005). Guiding of Relativistic Laser Pulses by Preformed Plasma Channels. *Phys. Rev. Lett.* **95**, 145002/1–4.

Gerestener, E. (2007). Physicists are planning lasers powerful enough to rip apart the fabric of space and time. *Nat.* **446**, 16–18.

Gibbon, P. (2005). *Short Pulse Laser Interactions with Matter, An Introduction*. London: Imperial College Press.

Glinec, Y., Faure, J., Pukhov, A., Kiselev, S., Gordienko, S., Mercier, B. & Malka, V. (2005). Generation of quasi-monoenergetic electron beams using ultrashort and ultraintense laser pulses. *Laser Part. Beams* **23**, 161–166.

Gordienko, S. & Pukhov, A. (2005). Scalings for ultrarelativistic laser plasmas and quasimonoenergetic electrons. *Phys. Plasmas* **12**, 043109/1-11.

Hegelich, B.M., Albright, B., Cobble, J., Flippo, K., Johnson, R., Letzring, S., Paffett, M., Ruhl, H., Schreiber, J., Schulze, R. & Fernandez, J.C. (2006). Mono-energetic multi-mev0nucleon ion beams accelerated by ultrahigh intensity lasers. *Nat.* **439**, 441–444.

Hemker, R.G., Hafz, N.M. & Uesaka, M. (2002). Computer simulations of a single-laser double-gas-jet wakefield accelerator concept. *Phys. Rev. St Accel. Beams* **5**, 041301/1-8.

Hidding, B., Amthor, K.-U., Liesfeld, B., Schwoerer, H., Karsch, S., Geissler, M., Veisz, L., Schmid, K., Gallacher, J.G., Jamison, S.P., Jaroszynski, D., Pretzler, G. & Sauerbrey, R. (2006). Generation of quasimono-energetic electron bunches with 80-fs laser pulses. *Phys. Rev. Lett.* **96**, 105004/1-4.

Hosokai, T., Kinoshita, K., Ohkubo, T., Maekawa, A., Uesaka, M., Zhidkov, A., Yamazaki, A., Kotaki, H., Kando, M., Nakajima, K., Bulanov, S.V., Tomassini, P., Giulietti, A. & Giuliett, D. (2006). Observation of strong correlation between quasimono-energetic electron beam generations by laser wakefield and laser guiding inside a preplasma cavity. *Phys. Lett. Rev. E* **73**, 036407/1-8.

Hutchinson, I. (1987). *Principles of Plasma Diagnostics*. Cambridge: Cambridge University Press.

Karmakar, A. & Pukhov, A. (2007). Collimated attosecond GeV electron bunches from ionization of high-Z material by radially polarized ultra-relativistic laser pulses. *Laser Part. Beams* **25**, 371–377.

Kostyukov, I., Pukhov, A. & Kiselev, S. (2004). Phenomenological theory of laser-plasma interaction in "bubble" regime. *Phys. Plasmas* **11**, 5256–5264.

Koyama, K., Adachi, M., Miura, E., Kato, S., Masuda, S., Watanabe, T., Ogata, A. & Tanimoto, M. (2006). Monoenergetic electron beam generation from a laser-plasma accelerator. *Laser Part. Beams* **24**, 95–100.

Leemans, W.P., Nagler, B., Gonsalves, A.J., Toth, C.S., Nakamura, K., Geddes, C.G.R., Esarey, E., Schroeder, C.B. & Hooker, S.M. (2006). GeV electron beams from a centimetre-scale accelerator. *Nat. Phys*. **2**, 696–699.

Lifschitz, A.F., Faure, J., Glinec, Y., Malka, V. & Mora, P. (2006). Proposed scheme for compact GeV laser plasma accelerator. *Laser Part. Beams* **24**, 255.

Malka, V., Fritzler, S., Lefebvre, E., Aleonard, M.M., Burgy, F., Chambaret, J.P., Chemin, J.F., Krushelnick, K., Malka, G., Mangles, S.P.D., Najmudin, Z., Pittman, M., Rousseau, J.P., Scheurer, J.N., Walton, B. & Dangor, A.E. (2002). Electron acceleration by a wakefield forced by an intense ultrashort laser pulse. *Sci.* **298**, 1596–1600.

Malka, V., Lifschitz, A., Faure, J. & Glinec, Y. (2006). Staged concept of laser-plasma acceleration toward multi-GeV electron beams. *Phys. Rev. Spe.Top. Acce. Beams* **9**, 091301/1-10.

Mangles, S.P.D., Thomas, A.G.R., Kaluza, M.C., Lundh, O., Lindau, F., Persson, A., Tsung, F.S., Najmudin, Z., Mori, W.B., Wahlstro, C.-G. & Krushelnick, K. (2006). Laser-wakefield acceleration of monoenergetic electron beams in the first plasma-wave period. *Phys. Rev. Lett*. **96**, 215001/1-4.

Marion, J.B. & Thornton, S.T. (1998). *Classical Dynamics of Particles and Systems*. Third Edition. New York: H.B.Jovanovich Pub.

Nickles, P.V., Ter-Avetisyan, S., Schnuerer, M., Sokollik, T., Sandner, W., Schreiber, J., Hilcher, D., Jahnke, U., Andreev, A. & Tikhonchuk, V. (2007). Review of ultrafast ion acceleration experiments in laser plasma at Max Born Institute. *Laser Part. Beams* **25**, 347–363.

Pukhov, A. & Meyer-Ter Vehn, J. (2002). Laser wakefield acceleration: The highly non-linear broken-wave regime. *Appl. Phys. B* **74**, 355–361.

Pukhov, A., Gordienko, S., Kiselev, S. & Kostyukov, I. (2004). The bubble regime of laser–plasma acceleration: Monoenergetic electrons and the scalability. *Plasma Phys. Contr. Fusion* **46**, B179–B186.

Robson, L., Simpson, P.T., Clarke, R.J., Ledingham, K.W.D., Lindau, F., Lundh, O., Mccanny, T., Mora, P., Neely, D., Wahlstro, C.-G., Zepf, M.M. & McKenna, P. (2007). Scaling of proton acceleration driven by petawatt-laser–plasma interactions. *Nat. Phys*. **3**, 58–62.

Roth, M., Brambrink, E., Audebert, P., Blazevic, A., Clarke, R., Cobble, J., Cowan, T.E., Fernandez, J., Fuchs, J., Geissel, M., Habs, D., Hegelich, M., Karsch, S., Ledingham, K., Neely, D., Ruhl, H., Schlegel, T. & Schreiber, J. (2005). Laser accelerated ions and electron transport in ultraintense laser matter interaction. *Laser Part. Beams* **23**, 95–100.

Ruhl, H., Cowan, T. & Pegoraro, F. (2006). The generation of images of surface structures by laser-accelerated protons. *Laser Part. Beams* **24**, 181–184.

Sadighi-Bonabi, R. & Kokabee, O. (2006). Evaluation of transmutation of $^{137}Cs(\gamma, n)^{136}Cs$ using ultra-intense laser in solid targets. *Chin. Phys. Lett*. **6**, 1434–1436.

Sadighi-Bonabi, R. & Zobdeh, P. (2008). Observation of quasi mono-energetic electron bunches in new ellipsoid cavity model. In *European Conference on Laser Interaction with Matter Proceedings*, Darmstadt, Germany: GSI.

Tanaka, K.A., Yabuuchi, T., Sato, T., Kodama, R., Kitagawa, Y., Takahashi, T., Ikeda, T., Honda, Y. & Okuda, S. (2005). Calibration of imaging plate for high energy electron spectrometer. *Rev. Sci. Inst*. **76**, 013507/1-5.

Tomassini, P., Galimberti, M., Giulietti, A., Giulietti, D., Gizzi, L.A., Labate, L. & Pegoraro, F. (2004). Laser wakefield acceleration with controlled self-injection by sharp density transition. *Laser Part. Beams* **22**, 423–429.

Umstadter, D. (2003). Relativistic laser–plasma interactions. *J. Phys. D: Appl. Phys*. **36**, R151–R165.

Yin, L., Albright, B.J., Hegelich, B.M. & Fernndez, J.C. (2006). GeV laser ion acceleration from ultrathin targets: The laser break-out afterburner. *Laser Part. Beams* **24**, 291–298.

Zobdeh, P., Sadighi-Bonabi, R. & Afarideh, H. (2009*a*). Cavity generation and effect of self-focusing in laser-plasma interaction. *Phys. Part. Nucl.* In press.

Zobdeh, P., Sadighi-Bonabi, R. & Afarideh, H. (2009*b*). Electron trajectory evaluation in laser-plasma interaction for effective output beam. *China Phys. B.* In press.

Zobdeh, P., Sadighi-Bonabi, R. & Afarideh, H. (2008*c*). New ellipsoid cavity model in the high intense laser-plasma interaction. *Plasma Dev. Operat*. **16**, 105–114.

Zobdeh, P., Sadighi-Bonabi, R., Afarideh, H., Yazdani, E. & Rezaei Nasirabad, R. (2008*d*). Using the steepened plasma profile and wave breaking threshold in laser-plasma interaction. *Contrib. Plasma Phys*. **48**, 555–560.